Acta Materialia 296 (2025) 121226

Contents lists available at ScienceDirect

Acta Materialia

journal homepage: www.elsevier.com/locate/actamat

Full length article

Predicting hydrogen storage properties of multicomponent metal hydrides: Modeling of pressure, capacity, hysteresis, and slope

Peter Hannappel [a,b,*], Marcus Vogt [a], Felix Heubner [a,*], Mateusz Balcerzak [a,c], Thomas Weißgärber [a,b]

[a] Fraunhofer Institute for Manufacturing Technology and Advanced Materials IFAM, Dresden Branch, Dresden, Germany
[b] TUD Dresden University of Technology, Faculty Mechanical Engineering, Institute of Materials Science, Chair Powder Metallurgy, Dresden, Germany
[c] Institute of Materials Science and Engineering, Poznan University of Technology, Poznań 61-138, Poland

ARTICLE INFO

Keywords:
Calphad thermodynamics
Ce-La-Ni-Al-Fe-Mn-H
Metal hydrides
PCI
Database

ABSTRACT

Metal hydrides are considered as an important group of materials in the future hydrogen-based economy. Their development is mostly based on time-consuming experimental trial-and-error methods. This work accelerates this pathway using a computational framework for the thermodynamic modeling of metal hydrides under para-equilibrium conditions. By employing the CALPHAD method on a six-component AB_5-type $(Ce, La)(Ni, Al, Fe, Mn)_5$–H system, we are able to make precise predictions regarding hydrogen absorption enthalpies, plateau pressures, and hydrogen sorption capacities. Additionally, this is the first time the hydrogenation/dehydroganation hysteresis effect has been successfully modeled using separate thermodynamic databases for hydrogen absorption and desorption. Furthermore, we introduce a method to directly calculate sloped pressure–composition–temperature (PCT) curves from X-ray diffraction data. This validation demonstrates the framework's capability to assess the hydrogen storage properties of complex multi-component systems in an efficient manner. This work lays the groundwork for future metal hydride thermodynamic studies on a variety of material classes, as well as optimization of alloys for applications even beyond classical hydrogen storage.

1. Introduction

Hydrogen plays a crucial role in the shift towards sustainable energy systems due to its clean energy potential and versatile applications. Nevertheless, the issue of efficient and safe hydrogen storage remains a significant challenge. Metal hydrides, such as AB_5-type alloys, offer a promising solution, enabling reversible hydrogen storage at reasonable pressures and temperatures [1–3]. The storage properties are critical because hydrogen storage must be feasible under conditions that align with practical applications, such as ambient or moderately elevated temperatures and pressures suitable for transportation and stationary applications. Moreover, metal hydrides have proven valuable in hydrogen compression, thermal management systems and hydrogen purification showcasing their versatility beyond classical storage applications [4,5]. By substituting elements on the A and B sites, the hydrogenation properties of AB_5-type alloys – including plateau pressures, hydrogen capacity, and reaction enthalpy – can be precisely tuned and therefore optimized for specific applications [2].

The necessity of modeling these sorption properties with computational tools is apparent from the considerable amount of recent research in this field [1,6]. The complex multi-component nature of metal hydrides presents a significant challenge in predicting their behavior. The CALPHAD (CALculation of PHAse Diagrams) method is a long-established approach for modeling and predicting the thermodynamic properties of such systems [7]. As it integrates both experimental data and thermodynamic principles, the incorporation of predictive tools such as density functional theory further enhances its capability for future advancements in the field. This combination allows for a substantial reduction in the experimental effort required to identify new alloy compositions and material classes for hydrogen applications, with the potential for a transformative impact on metal hydride-based research.

Recently, the authors published a computational tool to calculate the challenging para-equilibrium state and assess experimental data in a more automated procedure [8]. It was introduced on a basic ternary $(Ce,La)Ni_5$–H system. To further validate the proposed method, in the current work we chose the six-component $(Ce,La)(Ni,Al,Fe,Mn)_5$–H system, as it finds significant relevance in the metal hydride field and sufficient experimental data is present. Here we

* Corresponding authors.
E-mail addresses: peter.hannappel@ifam-dd.fraunhofer.de (P. Hannappel), felix.heubner@ifam-dd.fraunhofer.de (F. Heubner).

https://doi.org/10.1016/j.actamat.2025.121226
Received 6 February 2025; Received in revised form 28 May 2025; Accepted 6 June 2025
Available online 23 June 2025

focus on the important hydrogenation characteristics from a practical point of view. This includes the pressure–composition–temperature triplets (seen on an ideal stoichiometric alloy) and, for the first time, the prediction of pressure hysteresis between the absorption and desorption process as well as the plateau slope of non-stoichiometric alloys.

To address these challenges, this work includes the following contributions:

1. A step-by-step guide on modeling and predicting ideal hydrogenation properties of multi-component metal-hydride systems within the CALPHAD framework and the recently published program [8].
2. A novel approach to model the hysteresis of the absorption and desorption processes.
3. A new framework to incorporate X-ray diffraction (XRD) measurements into the CALPHAD method for predicting sloping plateaus.
4. Validation of the proposed methods on the (Ce,La)(Ni,Al,Fe,Mn)$_5$–H system.

2. Design process

2.1. Design parameters

To meet the diverse requirements of different applications of metal hydrides, a modeling tool needs to be able to predict and optimize a complex set of sorption properties. In our case, we want to optimize an alloy for a thermochemical systems. Therefore, we aimed to design an AB_5 alloy with the desired hydrogen sorption properties - a high hydrogen capacity together with a high reaction enthalpy. First we established the compositional boundaries for the AB_5 metal phase (excluding hydrogen) (see Table 1). Within these boundaries, we modeled key hydrogenation properties, including hydrogen capacity at specific pressures and temperatures, plateau pressure, and reaction enthalpy. Furthermore, coupling of this thermodynamic model with the phase stability limits allowed us to optimize the alloy compositions to achieve the desired hydrogen storage properties.

2.1.1. Stability of the AB_5 metal phase

The only stable binary alloys within the investigated (Ce,La)(Ni,Al,Fe,Mn)$_5$ system are $CeNi_5$ and $LaNi_5$. They both crystallize in the P6/mmm phase and are at room temperature approximately stoichiometric compounds [9]. La and Ce are fully soluble on the A site (in AB_5-type alloy), allowing complete substitution of one for the other [10]. Contrary to the A site elements, the substitution of Ni on the B site is limited in the ternary $LaNi_{5-x}M_x$ and $CeNi_{5-x}M_x$ phases (with M = Al, Fe, Mn). The boundaries for the B-side substitution of Ni were investigated thoroughly, elsewhere [2]. The substitutional limits of Al, Fe, and Mn in the $LaNi_{5-x}M_x$ phase are summarized in Table 1.

For the $CeNi_{5-x}Al_x$ system, the substitutional limits are reported to be higher than for the $LaNi_{5-x}Al_x$ system. Yamagishi et al. observed stable $CeNi_{5-x}Al_x$ alloys with x up to 2 [11]. Noticeably the lattice parameters have a discontinuity at around x = 1 to 1.25 and the hydrogenation properties start to degrade drastically. This means, although the $CeNi_{5-x}Al_x$ metal phase seems to have a higher solubility limit than the $LaNi_{5-x}Al_x$ phase, the hydride phase remains unstable above $CeNi_{3.75}Al_{1.25}H_x$. Due to the lack of available experimental data for the other $CeNi_{5-x}M_x$ systems and the inconsistencies reported in the $CeNi_{5-x}Al_x$ system, we leveraged the chemical similarity of La and Ce (for example similar ionic radii and electronic configuration) and develop the design rule based on the $LaNi_{5-x}M_x$ systems (Table 1). The substitutional limit x_{total} of a hypothetical multicomponent (Ce,La)$Ni_{5-x,i}M_{x,i}$ alloy with i components equals to

$$x_{\text{total}} = \sum_i \frac{x_i}{x_{\text{limit},i}} \tag{1}$$

Table 1
Experimental substitutional limits of elements M = Al, Fe, Mn in the metal phase $LaNi_{5-x}M_x$.

Element	Al	Fe	Mn
Substitutional limit x_{limit}	1.25 [12]	1.2 [13]	2 [14]

where x_i is the number of atoms per formula unit of the substitutional element i, and $x_{\text{limit},i}$ is the substitutional limit of this element. Thus, assuming a linear dependence of phase stability on x_{total}, any alloy composition with a substitutional element ratio resulting in $x_{\text{total}} \leq 1$ is expected to retain a stable, single-phase P6/mmm structure. Compositions with $x_{\text{total}} > 1$ will likely result in the formation of secondary phases. The formulation of Eq. (1) with the experimental values of Table 1 yields a composition of $Ce_xLa_{1-x}Ni_{3.59}Al_{0.47}Fe_{0.47}Mn_{0.47}$ (based on an equimolar ratio among the substitutional elements — Al, Fe, Mn), which approaches the threshold of $x_{\text{total}} = 1$. Any further increase in the substitutional element content beyond this composition would exceed the threshold and likely lead to the formation of secondary phases.

2.1.2. Thermodynamic modeling of the hydride phase

Within the defined substitutional limits of the metal phase the hydrogenated phase can be described by the hexagonal $P6_3mc$ structure [15]. To model the hydrogenation properties of the metal-hydrogen system, the Compound–Energy–Formalism within the CALPHAD framework was adopted [16]. The modeling process and the associated program were described in a previous paper by the authors [8]. In addition to the sorption properties that can be derived from the phase diagram (pressure–composition–temperature (PCT) triplets), the authors demonstrate a methodology for modeling the sloped PCT isotherms of non-stoichiometric compounds and the hysteresis of the absorption and desorption process (see below).

2.1.3. Ideal sorption properties

To establish a foundation for predicting the complete PCT curve, including hysteresis and slope characteristics, it is essential to first model the sorption properties of ideal, stoichiometric compounds.

The PCT relationship can be calculated by the partial equilibrium of the (temperature- and pressure-dependent) Gibbs energy curve of the metal-hydride phase and the hydrogen gas phase. The CALPHAD method extrapolates these equilibria from thermodynamic quantities: The enthalpy and entropy of formation, H_f and S_f, the mixing enthalpy H_{mix} and the configurational entropy S_{conf}, which are subsequently used to calculate the Gibbs energy curve for the metal-hydride phase G_{MH}:

$$G_{\text{MH}}(\mathbf{c},T) = H_f(\mathbf{c},T) - T\cdot S_f(\mathbf{c},T) + H_{\text{mix}}(\mathbf{c},T) - T\cdot S_{\text{conf}}(\mathbf{c},T) \tag{2}$$

Here, $\boldsymbol{c}$ represents the composition vector, consisting of the molar fractions of the metal elements and hydrogen.

The $AB_5(H,Va)_1(H,Va)_6$ sublattice model described by Hannappel et al. is used, as it shows good capabilities of modeling the sorption properties within the $Ce_{1-x}La_xNi_5$-H system [8,17,18]. Here, Va stands for vacancies and therefore (H,Va) is a hydrogen-vacancy sublattice.

The first assessment is done on experimental data, where absorption and desorption data are present. The logarithmic mean of the pressure values and the linear mean of the capacities are used to optimize the size and values of the thermodynamic database.

2.1.4. Hysteresis

Multiple theories for the origin of the differences between hydrogen absorption and desorption curves were developed. One of them, formulated by Schwarz and Khachaturyan, relates the hysteresis to an energetic barrier resulting from the elastic stresses created during the phase transition (from metallic phase to the hydride phase) [19]. This assumes that the E-Modulus and the mismatch in the unit cell sizes of the metal and hydride phase correlates directly with the hysteresis.

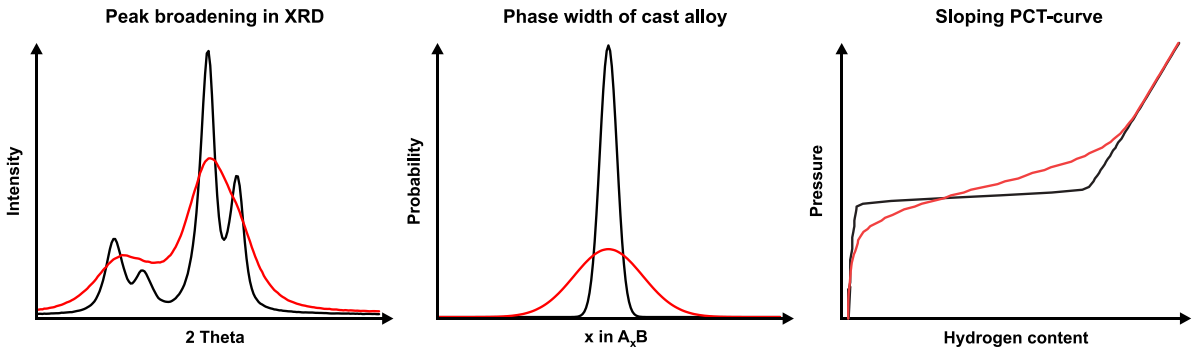

Fig. 1. Schematic representation of the proposed method for converting XRD microstrain data into sloped PCT curves. The diffraction angle-dependent peak broadening is correlated with microstrain, which is then converted into a Gaussian distribution of compositions (phase width, Eqs. (4)–(6)). Finally, the distribution of composition vectors is transformed into a sloped plateau by superimposing multiple ideal PCT curves (Eq. (8)).

In contrary, Flanagan and Clewley related the hysteresis to the inelastic stresses. In this case, dislocations must be formed due to the size mismatches during phase transition [20]. Therefore, the hysteresis scales with the number of dislocations and the formation enthalpy of the dislocations.

In any way, the different sorption pressures for absorption and desorption can be translated to a difference in the Gibbs energy for absorption and desorption:

$$\frac{1}{2}kT\ln\left(\frac{p_g^{\text{abs}}}{p_g^{\text{des}}}\right)=\frac{\delta G_{\text{abs}}}{\delta N_{\text{H}}}-\frac{\delta G_{\text{des}}}{\delta N_{\text{H}}} \tag{3}$$

Here, p_g is the partial pressure of the hydrogen gas and N_{H} is the amount of hydrogen in mole. The hysteresis can now be modeled with the CALPHAD method by generating two parameter sets that represent the Gibbs energy of the metal hydride during hydrogen absorption and desorption, G_{abs} and G_{des}, respectively. Elastic and inelastic stresses primarily affect the enthalpy due to the energy stored in lattice distortions and dislocation formation, which directly impact the Gibbs energy surface of the system. Therefore, we fix the entropy for both absorption and desorption to that of the standard entropy of hydrogen gas (130 J/mol-H_2K) and allow the enthalpy of formation and mixing enthalpy to be optimized between absorption and desorption [21].

While it is questionable whether a thermodynamic modeling tool can meaningfully predict kinetic effects, this is the first known attempt to use such a method. From a practical perspective, this approach allows to model the relevant observable sorption properties, and to select on this basis the optimized materials with predetermined hydrogen storage properties.

2.1.5. Plateau slope

The slope of the pressure plateau is an application-relevant sorption property. In many application scenarios, the slope significantly limits the usable capacity. The origin of the plateau slope is commonly attributed to a distribution of the alloy composition around the nominal stoichiometry [22]. This means the sloped plateau is a superposition of several plateaus corresponding to compositions slightly deviating from the nominal one. By extracting information about the microstrain distribution from XRD data and combining it with a thermodynamic model, the slope can be quantitatively predicted. Here, we briefly describe the method to get sloped PCT curves from XRD measurements, which is schematically shown in Fig. 1 and described in the following paragraphs.

According to the TOPAS reference manual [23], the refined microstrain parameter ϵ_0 obtained from the Double Voigt approach (cf. Materials and Methods section) is defined as the distribution width within which 50 % of the material's microstrain values are found. As long as the nominal alloy composition is not near a substitutional limit, it is reasonable to assume that the compositional distribution adheres to Gaussian statistics (as anisotropic microstrain broadening has not been observed). In Gaussian normal distributions, 50 % of the area under the curve lies within $\pm 0.6745\sigma$.

$$\epsilon_0=\frac{\Delta d}{d_0}=0.6745\cdot\sigma \tag{4}$$

Here, Δd is the distorted lattice parameter, d_0 is the lattice parameter of the nominal composition, and σ the standard deviation.

Microstrain is usually correlated to defects, such as vacancies, dislocations, or impurity atoms. With XRD measurements on the stoichiometric $LaNi_5$ and $CeNi_5$ compounds, the influence of dislocations on the peak broadening (introduced during alloy preparation) is quantified. This results in a correlation of the magnitude of the distorted lattice parameter with the phase width.

In the hexagonal unit cell of the P6/mmm phase, only the lattice parameters a and c are independent, with other parameters being constrained by symmetry. Therefore, ϵ_0 can be translated to a Gaussian distribution of the phase width PW with the boundary conditions:

$$\frac{\epsilon_{0,a}+\epsilon_{0,c}}{2}=\epsilon_0 \tag{5}$$

and

$$\sigma_{\text{PW}}(\epsilon_{0,a})=\sigma_{\text{PW}}(\epsilon_{0,c}) \tag{6}$$

In Chapter S1 of the Supplementary Information (SI), the dependence of the lattice parameters a and c on the chemical composition of the ternary systems is presented. From the ternary systems, we can extrapolate linearly to the mean change of the lattice parameter in dependence on the nominal composition:

$$\Delta d(\bar{x})=\frac{\sum_A\left(x_A\sum_{B\neq\text{Ni}}\left(x_B\Delta d(x_{A\text{Ni}_{5-x}B_x})\right)\right)+\sum_{A\neq\text{Ce}}\left(x_A\Delta d(x_{\text{Ce}_{1-x}\text{A}_x\text{Ni}_5})\right)}{\left(\sum_{A\neq\text{Ce},B\neq\text{Ni}}x_i\right)} \tag{7}$$

Here, x_i is the atomic fraction of the component i, on the A or B site, and $\Delta d(x_{\text{ternary}})$ is the change in the lattice parameter per atom change in the ternary systems, as summarized in Table 2. This equation results in a mean change of the lattice parameter a or c per mean atom $\bar{x}$. A detailed expression of this equation for the applied multi-component system is given in Chapter S1 in the SI.

Once the parameter σ_{PW} is determined, the sloping PCT curve is calculated by weighting the ideal stoichiometric PCT curves with the probabilities of the Gaussian function:

$$c_{\text{H}}=\sum_i c_{\text{H},i}\cdot p_i \tag{8}$$

where $c_{H,i}$ is the capacity of an ideal stoichiometric alloy with composition i, and p_i is the probability of the composition i within the distribution of the non-ideal alloy from Eq. (4).

Table 2
Extracted changes of the lattice parameters a and c of the ternary metal phases (also see Chapter S1 in SI).

System i	$\Delta d_{i,a}$	$\Delta d_{i,c}$
$LaNi_{5-x}Al_x$	0.04861	0.08745
$CeNi_{5-x}Al_x$	0.06906	0.07695
$LaNi_{5-x}Fe_x$	0.03478	0.03403
$LaNi_{5-x}Mn_x$	0.08046	0.08229
$CeNi_{5-x}Mn_x$	0.06229	0.07886
$Ce_{1-x}La_xNi_5$	0.12973	−0.02212

2.1.6. Review of existing experimental data

By extracting hydrogen sorption properties of quasi-binary ($CeNi_5$–H, $LaNi_5$–H) and quasi-ternary ($Ce_{1-x}La_xNi_5$–H, $LaNi_{5-x}M_x$–H, $CeNi_{5-x}M_x$–H) systems, the thermodynamic database is build. This database enables extrapolation to higher-order multicomponent systems.

A summary of the hydrogen sorption properties of the $(Ce,La)Ni_5$-H system has been made by Hannappel et al. [8]. The substitution of Al, Fe and Mn for Ni reduces the plateau pressure and the hydrogen storage capacity. Additionally, the substitution of Ni in the $La(Ni,Al,Fe,Mn)_5$ system increases the hysteresis. Contrary, in the $Ce(Ni,Al,Fe,Mn)_5$ system the substitution of Ni with Al, Fe and Mn is reducing the hysteresis [12,14,24,25].

PCT data for the optimization of two quasi-binary systems ($CeNi_5$–H and $LaNi_5$–H) and 5 ternary systems ($(La(Ni,Al)_5$–H, $Ce(Ni,Al)_5$–H, $La(Ni,Mn)_5$–H, $Ce(Ni,Mn)_5$–H, $La(Ni,Fe)_5$–H) were taken from the literature [8–12,14,24–34].

In the evaluated ternary systems within the $LaNi_{5-x}M_x$ – system, data over sufficient ranges of composition and temperature are available. For the complementary $CeNi_{5-x}M_x$ – system data is scarce. This is particularly critical for the $CeNi_{5-x}Fe_x$ – system, where no experimental data is available. While an option would be to take higher order systems into account for the optimization (e.g. the $Ce_{1-x}La_xNi_{5-y}Fe_y$ – system [32]) the current state of the assessment program does not include this functionality. Another possibility is to calculate the missing thermodynamic parameters from first-principle calculations. Because of the chemical similarity of Ce and La, the authors decided to mitigate this problem by choosing for the $CeNi_{5-x}Fe_x$ – system the same thermodynamic parameters as for the $LaNi_{5-x}Fe_x$ – system.

3. Materials and methods

The following synthesis and materials characterization were conducted to determine the proper experimental data for validating the predictions on the material properties, derived from the design process described in Section 2.

3.1. Material selection

Three material compositions were examined to validate the precision of the thermodynamic model in different positions in the $(Ce,La)(Ni,Al,Fe,Mn)_5$ compositional space. First, the model was used to find an alloy composition optimized to be used as a thermochemical heat source. Two boundary conditions were applied:

1. Plateau pressure during desorption at 333 K of 1 bar.
2. Maximize the enthalpy capacity during absorption.

The enthalpy capacity H_c is defined as

$$H_c = \Delta H \cdot n_{H_2,p} \tag{9}$$

Here, ΔH is the partial molar enthalpy of hydrogen in the plateau region in kJ/mol_{H2}, and $n_{H_2,p}$ is the hydrogen capacity at a certain pressure p in mol_{H2}/g_{metal}. The partial molar enthalpy of hydrogen can be calculated with the van't Hoff equation [35]. These boundary conditions yield an optimized Alloy_1 (see below) composition of $(Ce_{0.1}La_{0.9})(Ni_{4.47}Al_{0.06}Fe_{0.2}Mn_{0.27})$, with an enthalpy capacity of 0.21 kJ/g_{metal} at 40 bar.

Additionally, the boundaries of the model are evaluated by casting Alloy_2 and Alloy_3, which incorporate high amounts of B-side substitution elements Al, Fe, and Mn, with total substitution values of $x_{total} = 0.85$ for Alloy_2 and $x_{total} = 1.07$ for Alloy_3 (one alloy exceeding and one not exceeding the substitution threshold — see Eq. (1)).

In conclusion, three compositions are examined for validating the thermodynamic model within the $(Ce,La)(Ni,Al,Fe,Mn)_5$–H system:

1. $(Ce_{0.1}La_{0.9})(Ni_{4.47}Al_{0.06}Fe_{0.2}Mn_{0.27})$ ($H_c = 0.21$ kJ/g)
2. $(Ce_{0.65}La_{0.35})(Ni_{3.8}Al_{0.4}Fe_{0.4}Mn_{0.4})$ ($x_{total} = 0.85$)
3. $(Ce_{0.65}La_{0.35})(Ni_{3.5}Al_{0.5}Fe_{0.5}Mn_{0.5})$ ($x_{total} = 1.07$)

Each of the three compositions are evaluated in two states: as-cast and heat-treated. Therefore, a total of six distinct samples are examined in this study, labeled as Alloy_x_y, where x reflects the chemical composition number (1, 2 or 3) and y the alloy state (as-cast or heat-treated). This approach allows for comprehensive validation of the thermodynamic model within the $(Ce,La)(Ni,Al,Fe,Mn)_5$–H system.

3.2. Material synthesis

The samples were synthesized from high-purity elemental metals: Ce (99.9%, Osnabruegge GmbH), La (99.9%, VWR International GmbH), Ni (99.95%, Thermo Fisher GmbH), Al (99.9%, Thermo Fisher GmbH), Fe (99.97%, Thermo Fisher GmbH) and Mn (99.9%, Thermo Fisher GmbH). Metal pieces ranging from 1…10mm were used. The arc-melting method was employed under an argon atmosphere with an actively cooled Cu-crucible (AM500, Edmund Bühler GmbH). The metals were melted three times per side for two minutes and flipped in between.

Additionally, one-half of the as-cast samples were heat-treated under Argon atmosphere at 1273 K for 7 days (Alloy_x_heat-treated). The heat treatment leads to cast homogenization and, therefore, reduces the microstrain. These samples were used to examine the change of plateau slope due to the annealing process. The samples were stored and prepared in an inert argon atmosphere.

The single-phase crystal structure and oxygen impurities were proven with XRD analysis and Hot Gas Extraction (Fig. 4 and Supplementary Information, Section S2).

3.3. X-ray diffraction

XRD was conducted on as-cast and heat treated samples using Empyrean diffractometer (Malvern Panalytical GmbH, Mo-Kα-radiation ($\lambda_{K\alpha1} = 0.713609$ Å, $\lambda_{K\alpha2} = 0.709319$ Å), 2θ: 4–80 °, step size: 0.0072 °, time per step: 1600 s, Detector: Galipix 2D (Active length: 7.167 °), Anti-scatter slit: 1/2°, Divergence slit: 1/8°, Primary Soller slit: 0.02 rad, Secondary Soller slit: 0.04 rad) and the obtained data were analyzed using the Rietveld method.

Rietveld refinements of the diffraction data were performed using TOPAS 5 software [23] employing the fundamental parameters approach. All fundamental parameters were kept constant for different refinements. Crystallite size (CS) and strain microstructure effects (ϵ_0) were separated using the Double Voigt approach which utilizes convolutions of a Gaussian and Lorentzian profile function for both crystallite size and strain. Anisotropic microstructure broadening was negligible and therefore disregarded. To increase refinement reliabilities and differential precision of refined values, only a minimum set of variables

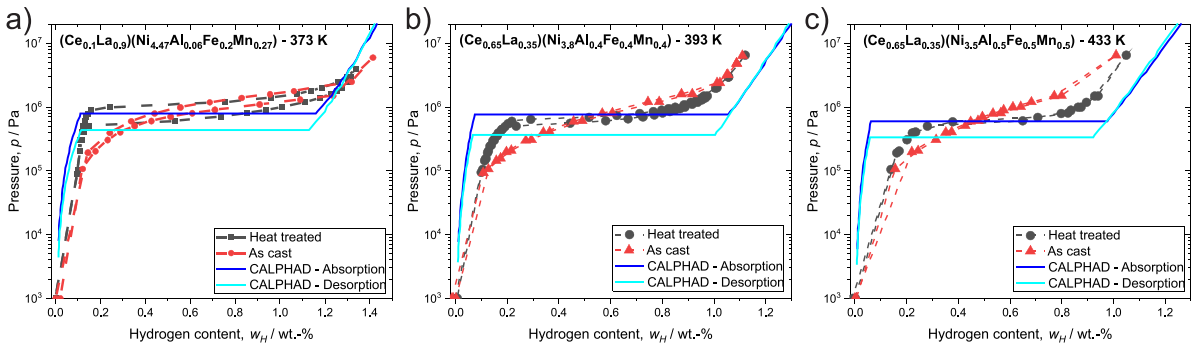

Fig. 2. Comparison of the CALPHAD model with the experimentally measured PCT curves for the as-cast and heat-treated samples for three alloy compositions: (a) Alloy_1 $Ce_{0.1}La_{0.9}(Ni_{4.47}Al_{0.06}Fe_{0.2}Mn_{0.27})$ – 373 K, (b) Alloy_2 $(Ce_{0.65}La_{0.35})(Ni_{3.8}Al_{0.4}Fe_{0.4}Mn_{0.4})$ – 393 K, (c) Alloy_3 $(Ce_{0.65}La_{0.35})(Ni_{3.5}Al_{0.5}Fe_{0.5}Mn_{0.5})$ – 433 K.

Table 3
Comparison of predicted and measured values for Alloy_1 – $(Ce_{0.1}La_{0.9})(Ni_{4.47}Al_{0.06}Fe_{0.2}Mn_{0.27})$ 373 K, Alloy_2 – $(Ce_{0.65}La_{0.35})(Ni_{3.8}Al_{0.4}Fe_{0.4}Mn_{0.4})$ 393 K and Alloy_3 – $(Ce_{0.65}La_{0.35})(Ni_{3.5}Al_{0.5}Fe_{0.5}Mn_{0.5})$ 433 K. The hysteresis factor was taken at the hydrogen content, where $p_{abs,as-cast} = p_{abs,ht}$. The values in brackets correspond to the relative error $\frac{|y_{model}-y_{exp}|}{y_{model}}$.

Composition	Capacity (at max. pressure) c_{max}/wt.%-H_2		Absorption pressure at $0.5 \cdot c_{max}$, p_{abs}/bar		Reaction enthalpy ΔH_{abs}/kJmol$^{-1}_{H2}$		Hysteresis factor $\ln(p_{abs}/p_{des})$	
	Experimental	Model	Experimental	Model	Experimental	Model	Experimental	Model
Alloy_1_as-cast	1.36 (4%)	1.31	11.5 (46%)	7.89	−31.3 (3%)	−32.11	0.33 (45%)	0.60
Alloy_1_heat-treated	1.33 (2%)		11.6 (47%)		−30.2 (6%)		0.54 (10%)	
Alloy_2_as-cast	1.11 (8%)	1.21	7.09 (8%)	7.71	−38.2 (4%)	−36.9	0.08 (89%)	0.73
Alloy_2_heat-treated	1.11 (8%)		7.66 (1%)		−36.5 (1%)		0.18 (75%)	
Alloy_3_as-cast	1.01 (13%)	1.16	7.20 (21%)	5.95	−39.3 (4%)	−40.9	0.04 (93%)	0.61
Alloy_3_heat-treated	1.05 (10%)		6.20 (4%)		−40.5 (1%)		0.06 (90%)	

was used for each refinement: 12 background parameters (Chebyshev polynomial), zero shift, lattice parameters, thermal parameters, 6 parameters to describe the preferred orientation of crystallites and scale factors. Site occupancies and atomic positions were kept fixed. All refinements were carefully checked for any parameter correlations. Any residual correlations between Gaussian contributions of strain and crystallite size were less or equal 62 % for all refinements. All other refined variables were correlated by less than 81 %. All refinements yielded good agreement between the observed and calculated patterns. χ^2 (R_{wp}/R_{exp}) of the refinements were between 5.30 and 6.95.

To introduce during preparation as little external strain as possible, the samples were manually ground in small batches and sieved with a 65 µm sieve. The material that passed through the sieve was collected, while the coarser fraction with the particle size remaining above 65 µm was carefully crushed and sieved again until 80 % of the material passed. Since this poses the risk of separating different phases, initial tests were conducted with and without sieving, and no phase separation was detected.

3.4. Sorption measurements

The samples were activated by alternating cycles of high (above plateau pressure) hydrogen pressure and vacuum at 293 K until no difference in the measured capacities could be observed. Between each cycle, the vacuum (10^{-3} Pa) was maintained for at least 30 min. Hydrogen sorption tests were conducted by detecting the weight differences during sorption. The threshold to define equilibrium was set as a mass change rate of 10 µg/min over a period of 10 min. This equals a relative mass change of 5×10^{-3} wt.% per minute. Each of the six Alloy_x_y were measured at three different temperatures. The experiments were performed up to 80 bar at different temperatures using a magnetic suspension balance (Waters GmbH). These experiments are used to calculate the reaction enthalpy by applying the van't Hoff equation. The sample preparation was done in air as a bulk piece of around 2 g.

4. Results and discussion

This chapter presents the results of modeling available experimental data (from the literature) using a recently published program [8]. Then the model predictions are evaluated with the properties of all six Alloy_x_y: in terms of pressure, capacity and reaction enthalpy. Last, the proposed technique to predict the pressure hysteresis and plateau slope is analyzed.

4.1. Modeling results

The digitized database is available in the supplementary material and in table format in Chapter S3 in the SI. A detailed comparison of the calculated sorption properties with the experimental training data is given in Figure S3 in the SI.

The seven evaluated systems ($CeNi_{5-x}M_x$ and $LaNi_{5-x}M_x$ (with M = Al, Fe, Mn) and $Ce_{1-x}La_xNi_5$) produced 4031 different parameter sets with a calculation effort of 22,394 core hours. The Arcaice Information Criterion algorithm to compensate for excessive use of interactive parameters results in a maximum of four interaction terms in the quasi-binary $LaAl_5$-H system and three interaction terms in the quasi-ternary $La(Ni,Al)_5$-H system. Contrarily for the $LaMn_5$-H, $CeMn_5$-H, $La(Ni,Mn)_5$-H and $Ce(Ni,Mn)_5$-H systems, only one interaction parameter is needed to represent each experimental data set. In total, 54 parameters were assessed to describe the 6-component system.

4.2. Prediction of PCT curves

The PCT curves for the six different Alloys_x_y are plotted in Fig. 2 The most important data has been summarized in Table 3 and visualized in Fig. 3. The results of hydrogen absorption/desorption experiments performed at other temperatures can be found in Chapter S4 the SI. As expected, the plateau pressures and hydrogen capacities are similar between the as-cast and heat-treated samples Fig. 2. The

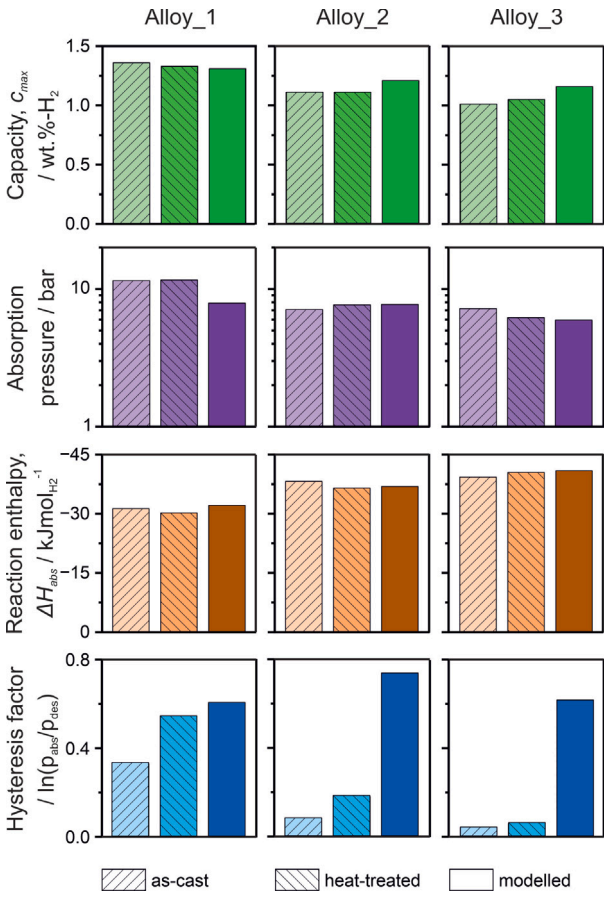

Fig. 3. Capacity, absorption pressure, reaction enthalpy and hysteresis factor measured and modeled for three studied alloys (in two stats: as-cast and heat-treated). Capacity and reaction enthalpy changes approximately linearly, while the plateau pressure changes exponentially with composition. The model is not predicting the diminishing hysteresis in the highly substituted samples (2–3).

main difference is the sloping of the PCT curve, which is much stronger for the as-cast samples than for the heat-treated ones.

Overall, the heat-treated samples show greater consistency with the CALPHAD model than the as-cast alloys. Although most of the experimental input data taken from literature is not annealed, the thermodynamic model predicts quantities regarding their thermodynamic (para-) equilibrium. Therefore, it is logical, that the annealed samples are closer to the equilibrated state.

The $(Ce_{0.1}La_{0.9})(Ni_{4.47}Al_{0.06}Fe_{0.2}Mn_{0.27})$ alloy samples (as-cast and heat-treated) with the lowest substitution content ($x_{total} = 0.53$) show the most precise results regarding the hydrogen capacity with a mean error of 3 % (see Table 3). The reaction enthalpy is predicted with a similar error. When looking at the target variable for Alloy_1, the enthalpy capacity H_c, we predicted this value with an accuracy of 1 % for the as-cast and 5 % for the heat-treated sample. This underlines the ability of the methodology, to predict alloys precisely for diverse hydrogen applications.

The prediction accuracy evolves differently for the distinct sorption properties, when going to higher amounts of substitutional elements (Alloy_2 and 3). The main strength of the computational method is the ability of modeling the plateau pressures. Even with substitution amounts close to the boundary of phase stability ($x_{total} \sim 1$), the errors of the predicted absorption pressures are very small. Especially for the heat-treated samples, which resemble the more equilibrated state, the errors for the $(Ce_{0.65}La_{0.35})(Ni_{3.8}Al_{0.4}Fe_{0.4}Mn_{0.4})$ and $(Ce_{0.65}La_{0.35})(Ni_{3.5}Al_{0.5}Fe_{0.5}Mn_{0.5})$ samples are 4 % and 1 %, respectively (see Table 3). The fact, that only binary interaction parameters are included for quasi-binary and -ternary systems underlines the ability of the CALPHAD method to extrapolate the sorption properties to higher-order systems.

The reaction enthalpy is deduced from the measurements of the absorption plateau pressures, which is why the prediction shows similar trends as for the absorption plateau pressures.

The error of the predicted hydrogen capacities is increasing with higher substitutional contents (2–4 % for $(Ce_{0.1}La_{0.9})(Ni_{4.47}Al_{0.06}Fe_{0.2}Mn_{0.27})$, 10–13 % for $(Ce_{0.65}La_{0.35})(Ni_{3.5}Al_{0.5}Fe_{0.5}Mn_{0.5})$, see Table 3). While the largest error is at 13 %, this trend underlines the observation made in our previous work, that modeling of the plateau boundaries (phase boundaries of the alpha and beta phase) is a much more difficult task [17].

The model for the AB_5 system was expanded to better represent the plateau boundaries, evolving from an $(A)(B)_5(H,Va)_7$ sublattice model [17,18] to an $(A)(B)_5(H,Va)_1(H,Va)_6$ configuration [8]. Possibly a more complex structure, where either the B side or the $(H,Va)_6$ site can be split into their distinct Wyckoff sites $6c_1$ and $6c_2$, could improve this capability even more. As the number of model parameters rises exponentially ($\sim 2^n$) with the increase of the number of sublattices n, while experimental data stays scarce, additional *ab initio* data is necessary to fill the parameters with physically meaningful quantities. Already with this sublattice model, the utilized parameter set is minimal compared to the vast parameter space, suggesting that the model may be overly complex and potentially overparameterized for the available data. Therefore, adding more hydrogen-vacancy sublattices will result in optimization problems due to overfitting.

4.3. Modeling of the pressure hysteresis

The best prediction regarding the pressure hysteresis shows the Alloy_1 with composition $(Ce_{0.1}La_{0.9})(Ni_{4.47}Al_{0.06}Fe_{0.2}Mn_{0.27})$ (Fig. 2a and Fig. 3) . Here, the heat-treated sample has an error of 10 % (see Table 3). In general, the heat-treated samples show a higher hysteresis factor, than the as-cast materials. It must be emphasized that the alloys have been properly activated until no changes in the PCT curves can be detected, as during the activation cycles the hysteresis can decrease. The cause of the hysteresis is still under debate, and these results emphasize the complex nature of this effect [36]. If the hysteresis would be purely an elastic effect, the model would yield proper results, as material properties such as the Young's modulus vary smoothly with composition and are in fact, thermodynamically modelable and therefore predictable [37].

With higher substitutional ratios the model does not reflect the decreasing hysteresis. It is astonishing that the highly substituted alloys yield hysteresis factors, that are more than a power of magnitude lower than of the low-hysteresis $LaNi_5$ alloy [10].

Our model predicts the hysteresis based on two different thermodynamical databases. This means, that besides the sublattice model and the parameter set, there is no physical connection between the two databases, which could also cause the random predictions. A more sophisticated model would include a hysteresis factor that is added to the reference Gibbs energy terms. Then, this term could be modeled and reflect changes due to temperature and composition. Furthermore, if the physical cause for the hysteresis effect can be found, thermodynamic quantities, for example, the bulk modulus, can be calculated with *ab initio* methods and integrated into a future model.

4.4. Modeling of the PCT curves slope

The results of the structural characterization of the as-cast and heat-treated alloys are summarized in Table 4. The diffraction profiles show a single P6/mmm structure for all of the compounds, indicating no secondary phases formed. Even for the compounds with a x_{total} slightly above 1, no other phase could be detected.

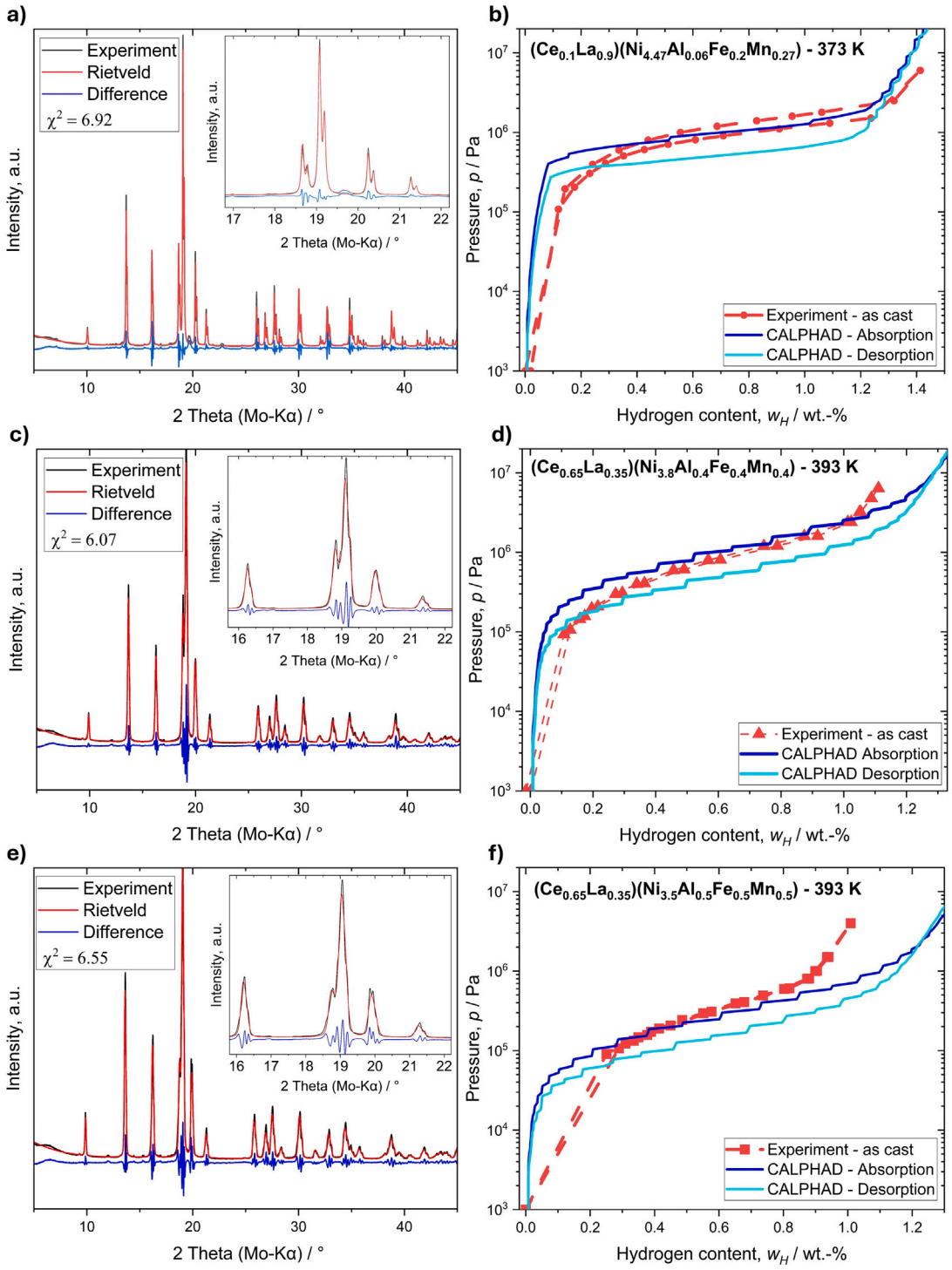

Fig. 4. Results of the X-ray experiments (a, c, e) and the corresponding PCT experiments (b, d, f) of the as-cast alloys: (a, b) Alloy_1 $(Ce_{0.1}La_{0.9})(Ni_{4.47}Al_{0.06}Fe_{0.2}Mn_{0.27})$, (c, d) Alloy_2 $(Ce_{0.65}La_{0.35})(Ni_{3.8}Al_{0.4}Fe_{0.4}Mn_{0.4})$, (e, f) Alloy_3 $(Ce_{0.65}La_{0.35})(Ni_{3.5}Al_{0.5}Fe_{0.5}Mn_{0.5})$. Insets show the parts of XRD patterns representing the most intensive reflections. On the right, the CALPHAD data is generated from the assessed database and the experimentally measured microstrain parameter.

The higher the concentration of substituent elements is, the higher the microstrain is (which is mainly an artifact of the phase width). The annealed samples show a reduction in the microstrain, likely dominated by the homogenization of the alloy.

In Fig. 4 and Figure S6 in the SI the result of the X-ray diffraction and sorption experiments are shown. The results show good agreement with the calculated PCT curves. The simulated slope is slightly smaller than experimentally measured in the PCT curves. In XRD measurements on the stoichiometric compounds $LaNi_5$ and $CeNi_5$ the influence of the dislocations on the microstrain was quantified to $\epsilon_{0,\mathrm{disl}} = 0.00006 - 0.00016$. As this effect was neglected in our model the difference of simulation to experiment would increase accordingly to the measured ϵ_0 values. This brings the conclusion, that other effects, such as kinetic limitations contribute to the sloping of the plateaus. The magnitude of this contribution can be approximated by the difference of the simulated and measured slopes in Fig. 4.

This result gives the opportunity, that with a single XRD measurement, the full non-ideal PCT curve of a metal alloy can be reasonably

Table 4
Extracted changes of the lattice parameters a and c of the ternary metal phases (also see Chapter S1 in SI).

Composition	a/Å	c/Å	ϵ_0
Alloy_1_as-cast	5.02837 (12)	4.01498 (12)	0.00083 (1)
Alloy_1_heat-treated	5.03060 (8)	4.02166 (7)	0.00039 (1)
Alloy_2_as-cast	4.99528 (17)	4.07742 (17)	0.00183 (2)
Alloy_2_heat-treated	4.99300 (3)	4.08130 (4)	0.00017 (2)
Alloy_3_as-cast	5.01271 (20)	4.09314 (19)	0.00191 (2)
Alloy_3_heat-treated	5.01462 (3)	4.09375 (3)	0.00016 (1)

well reconstructed. From the engineering point of view, this is a necessary information to assess the suitability of an alloy to a certain application.

5. Conclusions

This work establishes a crucial foundation for the thermodynamic modeling of metal hydrides under para-equilibrium conditions, demonstrating for the first time the successful integration of complex, multi-component metal-hydride systems into a coherent computational framework. The challenges associated with modeling the hydrogen sorption properties of metal hydrides, particularly under conditions of partial equilibrium, have been addressed through the development of a novel computational approach, introduced recently by the authors. The developed approach allows for the rapid assessment of many-component systems. In this paper, we validated the approach with precise predictions of reaction enthalpies, plateau pressures, and sorption capacities in a six-component system.

The implementation of different databases for absorption and desorption showed for the first time the capabilities representing the hysteresis effect with the CALPHAD method. Furthermore, the direct calculation of sloped PCT curves from X-ray diffraction data is another step in facilitating the development process of new hydrogen storage alloys. This paper contributes to addressing the ongoing questions about the origin of these non-ideal sorption properties. This work lies a foundation to model hysteresis between absorption and desorption. Our investigation emphasizes the need to link the two datasets with a physical component. Within our CALPHAD workflow, the sloping PCT is well reconstructed by the measurement of the phase width.

The methodology presented in this paper is not an endpoint but the beginning of a much broader application. This framework can be further expanded to other material systems, such as high-entropy-alloys, AB_2, and AB-type metal hydrides. Another necessary step to keep this modeling technique competitive with the increasing demand for predictive methods is to incorporate complementary computational tools. The usage of *ab initio* data can improve thermodynamic predictions where experimental data is scarce or difficult to obtain.

CRediT authorship contribution statement

Peter Hannappel: Writing – review & editing, Writing – original draft, Visualization, Validation, Software, Methodology, Investigation, Formal analysis, Data curation, Conceptualization. **Marcus Vogt:** Writing – review & editing, Software, Methodology. **Felix Heubner:** Writing – review & editing, Supervision, Funding acquisition, Conceptualization. **Mateusz Balcerzak:** Writing – review & editing, Visualization, Data curation. **Thomas Weißgärber:** Resources, Project administration, Funding acquisition.

Declaration of competing interest

The authors declare that they have no known competing financial interests or personal relationships that could have appeared to influence the work reported in this paper.

Acknowledgments

This work is part of the ThermOSS and HYPHAD projects.

Project HYPHAD was selected in the Joint Transnational Call 2023 of M-ERA.NET 3, which is an EU-funded network of about 49 funding organizations (Horizon 2020 grant agreement No 958174). The project is funded by the Korea Institute for Advancement of Technology, South Korea, the National Science Centre, Poland, and the Sächsisches Staatsministerium für Wissenschaft, Kultur und Tourismus, Germany. This project is co-financed with tax revenue on the basis of the budget adopted by the Saxon State Parliament. This research was financially supported by the Ministry of Trade, Industry and Energy (MOTIE) and Korea Institute for Advancement of Technology (KIAT) through the International Cooperative R&D program No. P0027799. This research was partially funded by the National Science Centre, Poland, number: 2023/05/Y/ST3/00249 under the M-ERA.NET 3 Call 2023.

Project ThermOSS is funded by the European Union and is co-financed with tax revenue on the basis of the budget adopted by the Saxon State Parliament.

The authors gratefully acknowledge the computing time made available to them on the high-performance computer at the NHR Center of TU Dresden. This center is jointly supported by the Federal Ministry of Education and Research (BMBF) and the state governments participating in the NHR.

Appendix A. Supplementary data

Supplementary material related to this article can be found online at https://doi.org/10.1016/j.actamat.2025.121226.

Data availability

The Electronic Supplementary Information attached to this article contains the raw and processed data necessary to reproduce the findings.

References

[1] N. Klopčič, I. Grimmer, F. Winkler, M. Sartory, A. Trattner, A review on metal hydride materials for hydrogen storage, J. Energy Storage 72 (2023) 108456, http://dx.doi.org/10.1016/j.est.2023.108456.

[2] J.-M. Joubert, V. Paul-Boncour, F. Cuevas, J. Zhang, M. Latroche, LaNi5 related AB5 compounds: Structure, properties and applications, J. Alloys Compd. 862 (2021) 158163, http://dx.doi.org/10.1016/j.jallcom.2020.158163.

[3] C. Pistidda, Solid-state hydrogen storage for a decarbonized society, Hydrogen 2 (4) (2021) 428–443, http://dx.doi.org/10.3390/hydrogen2040024.

[4] M. Lototskyy, V. Yartys, B. Pollet, R. Bowman, Metal hydride hydrogen compressors: A review, Int. J. Hydrog. Energy 39 (11) (2014) 5818–5851, http://dx.doi.org/10.1016/j.ijhydene.2014.01.158.

[5] B. Chandrakala, K. Sarath Babu, E. Anil Kumar, Thermodynamic analysis of La and Mm based metal hydride pairs for solar energy-driven cold storage applications, Therm. Sci. Eng. Prog. 50 (2024) 102548, http://dx.doi.org/10.1016/j.tsep.2024.102548.

[6] K. Nivedhitha, T. Beena, N. Banapurmath, M. Umarfarooq, V. Ramasamy, M.E.M. Soudagar, Ü. Ağbulut, Advances in hydrogen storage with metal hydrides: Mechanisms, materials, and challenges, Int. J. Hydrog. Energy 61 (2024) 1259–1273, http://dx.doi.org/10.1016/j.ijhydene.2024.02.335, URL https://www.sciencedirect.com/science/article/pii/S036031992400778X.

[7] Z.-K. Liu, Thermodynamics and its prediction and CALPHAD modeling: Review, state of the art, and perspectives, Calphad 82 (2023) 102580, http://dx.doi.org/10.1016/j.calphad.2023.102580, URL https://www.sciencedirect.com/science/article/pii/S0364591623000524.

[8] P. Hannappel, F. Heubner, M. Balcerzak, T. Weißgärber, Advancing the thermodynamic modeling of multicomponent phases in hydrogen-para-equilibrium, Acta Mater. 284 (2025) 120529, http://dx.doi.org/10.1016/j.actamat.2024.120529, URL https://www.sciencedirect.com/science/article/pii/S1359645424008784.

[9] H. Senoh, N. Takeichi, H.T. Takeshita, H. Tanaka, T. Kiyobayashi, N. Kuriyama, Hydrogenation properties of RNi5 (R: rare earth) intermetallic compounds with multi pressure plateaux, Mater. Trans. 44 (9) (2003) 1663–1666, http://dx.doi.org/10.2320/matertrans.44.1663.

[10] P. Zhou, J. Zhang, J. Bi, X. Xiao, Z. Cao, L. Zhan, H. Shen, M. Lu, Z. Li, Y. Zhao, L. Wang, M. Yan, L. Chen, Underlying factors of mega pressure hysteresis in cerium-rich CaCu5-type metal hydrides and effective modification strategies, J. Mater. Chem. A 11 (2023) 25963–25972, http://dx.doi.org/10.1039/D3TA06351H.

[11] R. Yamagishi, T. Kojima, S. Kameoka, D. Okuyama, T.J. Sato, C. Nishimura, A.-P. Tsai, Creating the hydrogen absorption capability of CeNi5 through the addition of Al, Int. J. Hydrog. Energy 42 (34) (2017) 21832–21840, http://dx.doi.org/10.1016/j.ijhydene.2017.07.072.

[12] H. Diaz, A. Percheron-Guégan, J. Achard, C. Chatillon, J. Mathieu, Thermodynamic and structural properties of LaNi5-yAly compounds and their related hydrides, Int. J. Hydrog. Energy 4 (5) (1979) 445–454, http://dx.doi.org/10.1016/0360-3199(79)90104-6.

[13] J. Lamloumi, A. Percheron-Guegan, J. Achard, G. Jehanno, D. Givord, Study of the pseudobinary compounds LaNi5-x fe x (x ≤ 1.2) by X-ray diffraction, mössbauer spectroscopy and magnetic measurements, J. Phys. Fr. 45 (10) (1984) 1643–1652, http://dx.doi.org/10.1051/jphys:0198400450100164300.

[14] C. Lartigue, A. Percheron-Guégan, J. Achard, F. Tasset, Thermodynamic and structural properties of LaNi5-xMnx compounds and their related hydrides, J. the Less Common Met. 75 (1) (1980) 23–29, http://dx.doi.org/10.1016/0022-5088(80)90365-3, URL https://www.sciencedirect.com/science/article/pii/0022508880903653.

[15] A. Al Alam, S. Matar, M. Nakhl, N.O. ni, Investigation of changes in crystal and electronic structures by hydrogen within LaNi5 from first-principles, Solid State Sci. 11 (6) (2009) 1098–1106, http://dx.doi.org/10.1016/j.solidstatesciences.2009.02.026.

[16] M. Hillert, The compound energy formalism, J. Alloys Compd. 320 (2) (2001) 161–176, http://dx.doi.org/10.1016/S0925-8388(00)01481-X, Materials Constitution and Thermochemistry. Examples of Methods, Measurements and Applications. In Memoriam Alan Prince.

[17] P. Hannappel, E. Alvares, F. Heubner, C. Pistidda, P. Jerabek, T. Weißgärber, Thermodynamic assessment of the CeH and CeNi5 H system, Calphad 85 (2024) 102701, http://dx.doi.org/10.1016/j.calphad.2024.102701.

[18] M. Palumbo, J. Urgnani, D. Baldissin, L. Battezzati, M. Baricco, Thermodynamic assessment of the H–La–Ni system, Calphad 33 (1) (2009) 162–169, http://dx.doi.org/10.1016/j.calphad.2008.09.003.

[19] R.B. Schwarz, A.G. Khachaturyan, Thermodynamics of open two-phase systems with coherent interfaces: Application to metal–hydrogen systems, Acta Mater. 54 (2) (2006) 313–323, http://dx.doi.org/10.1016/j.actamat.2005.08.044.

[20] T.B. Flanagan, W. Luo, J. Clewley, Calorimetric enthalpies of absorption and desorption of protium and deuterium by palladium, J. Less Common Met. 172–174 (1991) 42–55, http://dx.doi.org/10.1016/0022-5088(91)90431-3.

[21] J.-M. Joubert, CALPHAD modeling of metal–hydrogen systems: A review, JOM 64 (12) (2012) 1438–1447, http://dx.doi.org/10.1007/s11837-012-0462-6.

[22] C.-N. Park, S. Luo, T.B. Flanagan, Analysis of sloping plateaux in alloys and intermetallic hydrides: I. Diagnostic features, J. Alloys Compd. 384 (1) (2004) 203–207, http://dx.doi.org/10.1016/j.jallcom.2004.04.101, URL https://www.sciencedirect.com/science/article/pii/S0925838804006097.

[23] A.A. Coelho, *TOPAS* and *TOPAS-Academic*: an optimization program integrating computer algebra and crystallographic objects written in C++, J. Appl. Crystallogr. 51 (1) (2018) 210–218, http://dx.doi.org/10.1107/S1600576718000183.

[24] J. Lamloumi, A. Percheron-Guegan, C. Lartigue, J. Achard, G. Jehanno, Thermodynamic, structural and magnetic properties of LaNi5 - xFex hydrides, J. the Less Common Met. 130 (1987) 111–122, http://dx.doi.org/10.1016/0022-5088(87)90093-2, URL https://www.sciencedirect.com/science/article/pii/0022508887900932 Proceedings of the International Symposium on the Properties and Applications of Metal Vydrides V.

[25] F. Pourarian, W. Wallace, The effect of substitution of Mn or Al on the hydrogen sorption characteristics of CeNi5, Int. J. Hydrog. Energy 10 (1) (1985) 49–58, http://dx.doi.org/10.1016/0360-3199(85)90135-1, URL https://www.sciencedirect.com/science/article/pii/0360319985901351.

[26] E.R. Pinatel, M. Palumbo, F. Massimino, P. Rizzi, M. Baricco, Hydrogen sorption in the LaNi5-xAlx-H system (0 ≤ x ≤ 1), Intermetallics 62 (2015) 7–16, http://dx.doi.org/10.1016/j.intermet.2015.03.002.

[27] T. Kodama, The thermodynamic parameters for the LaNi5-xAlx–H2 and MmNi5-xAlx–H2 systems, J. Alloys Compd. 289 (1) (1999) 207–212, http://dx.doi.org/10.1016/S0925-8388(99)00173-5.

[28] A.N. Kazakov, I.A. Romanov, A.V. Bezdudny, A.A. Eronin, D.V. Blinov, Low temperature AB5 alloys for thermal energy storage systems, Int. J. Hydrog. Energy 58 (2024) 627–632, http://dx.doi.org/10.1016/j.ijhydene.2024.01.242.

[29] S. Luo, J. Clewley, T.B. Flanagan, R. Bowman, L. Wade, Further studies of the isotherms of LaNi5-xSnx–H for x=0–0.5, J. Alloys Compd. 267 (1) (1998) 171–181, http://dx.doi.org/10.1016/S0925-8388(97)00536-7.

[30] V.K. Sharma, E. Anil Kumar, Effect of measurement parameters on thermodynamic properties of La-based metal hydrides, Int. J. Hydrog. Energy 39 (11) (2014) 5888–5898, http://dx.doi.org/10.1016/j.ijhydene.2014.01.174.

[31] H. Dhaou, F. Askri, M. Ben Salah, A. Jemni, S. Ben Nasrallah, J. Lamloumi, Measurement and modelling of kinetics of hydrogen sorption by LaNi5 and two related pseudobinary compounds, Int. J. Hydrog. Energy 32 (5) (2007) 576–587, http://dx.doi.org/10.1016/j.ijhydene.2006.07.001.

[32] W.-l. Mi, Z.-s. Liu, T. Kimura, A. Kamegawa, H.-l. Wang, Crystal structure and hydrogen storage properties of (La,Ce)Ni5−xMx (M=Al, Fe, or Co) alloys, Int. J. Miner. Met. Mater. 26 (1) (2019) 108–113, http://dx.doi.org/10.1007/s12613-019-1714-z.

[33] J.F. Lakner, T.S. Chow, Hydrides of $CeNi_5$, $MmNi_5$, $Ca_{0.2}(Ce_{0.65}Mm_{0.35})_{0.8}Ni_5$, $Ca_{0.2}Ce_{0.8}Ni_5$, $Ca_{0.2}Mm_{0.8}Ni_5$, and Mixed $CeNi_5$/$MmNi_5$, Report, University of North Texas Libraries, UNT Digital Library, 1982, URL https://digital.library.unt.edu/ark:/67531/metadc1212316/, (Accessed 5 January 2024).

[34] S. Klyamkin, V. Verbetsky, A. Karih, Thermodynamic particularities of some CeNi5-based metal hydride systems with high dissociation pressure, J. Alloys Compd. 231 (1) (1995) 479–482, http://dx.doi.org/10.1016/0925-8388(95)01869-7.

[35] C. Rongeat, I. Llamas-Jansa, S. Doppiu, S. Deledda, A. Borgschulte, L. Schultz, O. Gutfleisch, Determination of the heat of hydride formation/decomposition by high-pressure differential scanning calorimetry (HP-DSC), J. Phys. Chem. B 111 (46) (2007) 13301–13306, http://dx.doi.org/10.1021/jp075954r, PMID: 17973422.

[36] N.J. Weadock, P.W. Voorhees, B. Fultz, Interface pinning causes the hysteresis of the hydride transformation in binary metal hydrides, Phys. Rev. Mater. 5 (1) (2021) http://dx.doi.org/10.1103/PhysRevMaterials.5.013604.

[37] J. Ling, Z. Wen, G. Yang, Y. Wang, W. Chen, A CALPHAD-type Young's modulus database of ti-rich Ti–Nb–Zr–Mo system, Calphad 73 (2021) 102255, http://dx.doi.org/10.1016/j.calphad.2021.102255, URL https://www.sciencedirect.com/science/article/pii/S0364591621000067.